Acoustic scattering from fluid-loaded elastic shells: A Gaussian beam approach

Yang Yanga)

SFA, Inc., 1401 McCormick Drive, Landover, Maryland 20785

Andrew N. Norris

Department of Mechanical and Aerospace Engineering, Rutgers University, Piscataway, New Jersey 08855-0909

Luise S. Couchman

Code 7131, U.S. Naval Research Laboratory, Washington, DC 20375-5000

(Received 7 November 1994; accepted for publication 30 January 1995)

A new method is described for computing the acoustic far field scattered by a submerged smooth elastic thin shell. The total field is split into a sum of specular and leaky wave contributions. The latter arise from weakly radiating membrane waves that propagate globally over the structure, and are the focus of this work. The scattered leaky wave field is expressed, via a surface Helmholtz integral, as the sum of integrals along a finite number of Gaussian beams. The integral on each beam is then approximated as a line integral along the central ray of the beam. Finally, the far-field contribution from each line integral is reduced to a sum of stationary phase contributions. The derived asymptotic expression for the leaky wave field is uniformly valid for all observation directions. Difficulties associated with caustics and two-point ray tracing do not arise in the present formalism. A test of the method for a spherical shell shows that the numerical results agree well with the exact solution and the pure ray solution for $k_f a > 10$, where k_f is the fluid wave number. © 1995 Acoustical Society of America.

PACS numbers: 43.20.Dk, 43.20.Fn, 43.30.Gv. 43.40.Rj

INTRODUCTION

Acoustic scattering problems for fluid-loaded elastic shells are usually formulated in terms of surface Helmholtz integrals. The direct evaluation of these surface integrals at high frequencies is a formidable task because the required computational time increases substantially with frequency. In contrast, ray-based approaches are best suited to the higher frequencies, and provide the natural means for dealing with this regime. From the ray point of view, the scattered field at a distant observation point is dominated by the surface field at a few distinct points on the shell, the so-called launching points. Apart from the point of specular reflection, which is relatively easy to predict and handle, the dominant mechanism for radiation from the launch points is by supersonic "membrane" wave motion. Therefore in order to obtain the associated membrane wave scattered field, one needs to determine (i) the field at the coupling points where the incident rays couple to the membrane rays on the shell's surface, (ii) the ray paths from the coupling points to the launching points, and (iii) the field at the launching points. This interpretation has lead to enormous insight into the mechanism of wave scattering and radiating from submerged elastic shells, and has resulted in considerable simplification. However, the determination of the field at the launching points often turns out to be nontrivial because it usually involves twopoint ray tracing. In a traditional ray theory the surface wave field is defined only along the rays, and the field at a launching point depends on those rays that pass exactly through it. Searching for these rays from all possible rays by a twopoint ray tracing method could be computationally costly, and may be unrealistic, except for simple shells such as spheres and cylinders where the ray paths are well known.

Some modifications to the "traditional" ray method seem to be necessary in order to use it for constructing the field scattered by an arbitrarily curved shell. A natural approach is the paraxial approximation of the wave field in the vicinity of a ray, which is often called the Gaussian beam method. A Gaussian beam may be considered as a bundle of rays in complex space in the neighborhood of the central ray, which is in real space. The field along the beam is concentrated in the vicinity of its central ray, and the amplitude on the cross section of the beam has a Gaussian profile. The trajectory of the beam is described by its central ray path, which can be determined by the pure ray method. In comparison with the pure ray method, there are two major advantages to be gained by using the Gaussian beam method for the propagation and radiation of waves on a curved shell. First, a Gaussian beam is always finite at caustics so that the surface field synthesized from all the beams is well defined at every point on the surface, and there is no need to determine caustic locations. Second, the Gaussian beam method is more efficient than the ray method because two-point ray tracing is not required.

The Gaussian beam method has had wide use in wave propagation and scattering problems. The earlier applications can be traced back to the papers of Keller and Streifer,² Deschamps,³ and Felsen.⁴ The Gaussian beam technique has been extensively exploited in geophysics in the last decade

^{a)}Under contract to U.S. Naval Research Laboratory, Washington, DC 20375-5000.

by Červený et al., ⁵ Nowack and Aki, ⁶ and Norris et al. ⁷ Most applications of this technique, however, are limited to three-dimensional Euclidean space. Due to the geometrical complexity, the Gaussian beam method to date has not been directly applied to the construction of the acoustic field scattered by an arbitrarily curved shell.

The objective of this paper is to determine the acoustic field scattered by a submerged shell of arbitrary smooth shape through the use of the Gaussian beam method. The principal assumption employed is that elastic wavelengths are much greater than the shell thickness but much smaller than the principal radii of curvature defined over the shell's surface. Consequently, thin shell theory and high-frequency asymptotics are directly applicable. The paper is organized as follows. Membrane ray theory for thin elastic shells, developed by Norris and Rebinsky, 1,8,9 is briefly reviewed in Sec. I. Gaussian beams are introduced and some of their basic properties on a curved surface are discussed in detail. In Sec. II, the surface integral for the scattered field is approximated by a sum of Gaussian beams, and an explicit asymptotic expression for the scattered field is derived. A numerical scheme is described in Sec. III which combines the Gaussian beam method with the pure ray method. The scheme is explicitly tested against the available analytical solutions for a submerged spherical shell. Numerical results for the acoustic far field are discussed in Sec. III.

I. RAYS AND BEAMS ON A CURVED SURFACE

The essence of the Gaussian beam summation method is to approximate the wave field by a number of Gaussian beams, each of which is exponentially localized in the vicinity of its central ray. The central rays form the framework upon which the Gaussian beams are patched and the trajectories of the central rays are determined by the pure ray method. The foundation of the Gaussian beam approach is therefore pure and simple ray theory. We will first summarize the pertinent aspects of ray theory for thin elastic shells, and then discuss solutions in the form of Gaussian beams.

A. Review of membrane ray theory

The geometry of a smooth shell's surface of arbitrary shape, Σ , can be described by two families of curvilinear coordinate curves ξ^1 and ξ^2 on Σ . The position vector at a point (ξ^1, ξ^2) is written as

$$\mathbf{x} = \mathbf{x}(\xi^1, \xi^2). \tag{1}$$

Consider a plane acoustic wave incident upon Σ in the direction \mathbf{n}^{in} . The wave is not only reflected in a normal or "specular" manner by the shell's surface but may also excite shell membrane waves at points where the phase of the incident wave matches to that of the membrane waves. The term "membrane wave" is used here to denote supersonic waves with displacements predominantly in the surface. They have been discussed in detail by, for example, Norris and Rebinsky. The polarization of the waves leads to weak coupling with the fluid and hence the membrane waves are only weakly radiating, or leaky. To a first approximation, the phase matching condition is

$$\mathbf{n}^{\text{in}} \cdot \mathbf{a}_3 = -\cos \theta_0$$
, $\sin \theta_0 = k/k_f$, (2)

where a_3 is the unit outward normal to Σ , θ_0 is the critical angle for the membrane wave, k_f is the acoustic wave number, and k the membrane wave number. The roots of Eq. (2)₁ define the starting points, or the coupling points, for all the excited membrane rays. An efficient numerical scheme was recently developed by Yang *et al.*¹⁰ to determine the coupling points on arbitrarily curved shells. The set of coupling points for each type of membrane wave form a closed curve on a smooth shell, viz., the coupling curve.

The membrane wave number k is a root of the dispersion relation for the submerged shell. The relation was first derived by Pierce, ¹¹ and was further simplified by Norris and Rebinsky^{8,9} in the limit $k_f R_{\min} \gg 1$, where R_{\min} is the smallest radius of the curvature on the shell's surface. The asymptotic approximation to the root may be written as¹

$$k^{2} \approx \frac{\omega^{2}}{c^{2}} + (1 - \nu)K - \frac{Z_{m}}{Z_{m} + Z_{s}} \frac{1}{R_{0}^{2}},$$
 (3)

where c is the phase speed associated with straight-crested waves on a flat plate: $c = c_p$ for longitudinal waves, or $c = c_t$ for transverse waves. The impedances in Eq. (3) are

$$Z_m = -i\omega\rho_s h$$
, $Z_s = Z_f(\theta_0)$, $Z_f(\theta) = \rho_f c_f \sec \theta$, (4)

where h is the thickness, and ρ_s and ρ_f are the densities of the shell and the surrounding fluid. The parameter R_0 is the dynamic effective local radius of curvature, defined by

$$\frac{1}{R_0} = \begin{cases} 1/R_{\parallel} + \nu/R_{\perp} , & \text{longitudinal,} \\ 2/R_T, & \text{transverse,} \end{cases}$$
 (5)

with

$$\frac{1}{R_{\parallel}} = n^{\alpha} d_{\alpha\beta} n^{\beta}, \quad \frac{1}{R_{\perp}} = n^{\perp \alpha} d_{\alpha\beta} n^{\perp \beta},$$

$$\frac{1}{R_{T}} = \frac{1}{2} \left(n^{\alpha} d_{\alpha\beta} n^{\perp \beta} + n^{\perp \alpha} d_{\alpha\beta} n^{\beta} \right).$$
(6)

The unit vectors \mathbf{n} and \mathbf{n}^{\perp} lie in Σ , parallel and perpendicular to the surface ray direction, respectively. The surface curvature tensor is $d_{\alpha\beta}$ and K is the Gaussian curvature,

$$K = \frac{1}{R_{\parallel}R_{\perp}} - \frac{1}{R_T^2}. (7)$$

Note that the final term in Eq. (3) is complex, and its imaginary part accounts for the attenuation of the membrane waves through radiation loss. Although $k_f R_{\min} \gg 1$ is assumed and consequently the leading-order term in Eq. (3) is much larger than the others, one must include the fluid-loading term in the dispersion equation even in the first-order approximation; otherwise there is no attenuation. Our approach therefore is to retain the fluid-loading term in Eq. (3) when we evaluate the global phase variation (and resulting radiation loss) as the ray propagates over the shell, but ignore the fluid-loading term in the computations of the coupling curve, the ray trajectories, and the ray tube widths.

The leading-order approximation to the ray trajectories therefore follow from Eq. (3) as the characteristic curves of the eikonal equation

$$k^2 = \omega^2/c^2$$
, or $\nabla \phi_s \cdot \nabla \phi_s = 1/c^2$, (8)

where k is the magnitude of the surface wave-number vector,

$$\mathbf{k} = \omega \nabla \phi_{s} = k\mathbf{n},\tag{9}$$

and $\phi_s(\mathbf{x})$ is the timelike phase function on Σ . Furthermore, on a shell of homogeneous material and thickness, the membrane wave speed is approximately constant over the entire surface Σ . Thus to leading order the rays describe geodesic paths on Σ . Let s be arc length along a ray; then (ξ, ξ^2) satisfy the well-known differential equations

$$\frac{d\xi^{\alpha}}{ds} = n^{\alpha}, \quad \frac{dn^{\alpha}}{ds} = -\Gamma^{\alpha}_{\beta\gamma}n^{\beta}n^{\gamma}, \tag{10}$$

where $\Gamma^{\alpha}_{\beta\gamma}$ are the Christoffel symbols of the second kind. ¹² The ray trajectories are uniquely determined by solving these equations with initial conditions prescribed on the coupling curve \mathscr{C} ,

$$\xi^{\alpha}(0) = \xi^{\alpha}|_{\mathcal{C}}, \quad \mathbf{n}(0) = \csc \theta_0 (\mathbf{n}^{\mathsf{in}} - (\mathbf{n}^{\mathsf{in}} \cdot \mathbf{a}_3) \mathbf{a}_3)|_{\mathcal{C}}.$$
(11)

The ray tube width A(s) is a measure of the spreading between neighboring rays. The differential equations for A follow from Eq. (10) by taking variations with respect to a parameter r along the direction \mathbf{n}^{\perp} . The resulting equations, or the variational ray equations, are

$$\frac{dA}{ds} = cB, \quad c\frac{dB}{ds} = -KA. \tag{12}$$

It has been shown by Norris⁹ that the wavefront curvature on the shell's surface is the quotient of B(s) and A(s),

$$\mu(s) \equiv n^{\perp \alpha} n^{\perp \beta} \nabla_{\alpha} \nabla_{\beta} \phi_s = B(s)/A(s). \tag{13}$$

The value of A(0) is arbitrary, and may be set to unity with no loss in generality. The initial wavefront curvature is then B(0), which is derived by local phase matching between the incident and surface waves at the coupling point. In short,

$$A(0)=1$$
, $B(0)=\mu(0)=c^{-1}\cot\theta_0 KR_1|_{\mathcal{L}}$. (14)

One may directly solve Eqs. (12) using the initial condition (14). Alternatively, the general solution can be written as a linear combination of two independent solutions, (A_1,B_1) and (A_2,B_2) , to Eqs. (12):

$$A(s) = A_1(s) + \mu(0)A_2(s), \tag{15}$$

$$B(s) = B_1(s) + \mu(0)B_2(s)$$

with initial conditions

$$A_1(0) = B_2(0) = 1, \quad B_1(0) = A_2(0) = 0.$$
 (16)

Using Eqs. (12) and the initial conditions (14), one can show that the Wronskian, or Lagrange ray invariant, ¹³ is constant and equal to unity along the entire ray trajectory; that is,

$$A_1(s)B_2(s) - A_2(s)B_1(s) = 1.$$
 (17)

The membrane wave displacement amplitude V(s) satisfies the simplified transport equation¹

$$\frac{d}{ds}\left(V\sqrt{\rho_s hcA}\right) = 0. \tag{18}$$

Assuming uniform material properties, we then have

$$V(s) = V(0) \left(\frac{A(0)}{A(s)}\right)^{1/2},\tag{19}$$

where the initial amplitude is1

$$V(0) = \frac{-P_0}{i\omega k R_0} \frac{(i2\pi k R_1 \tan \theta_0)^{1/2}}{Z_m + Z_s},$$
 (20)

and P_0 is the amplitude of the incident acoustic wave. The surface pressure generated by a membrane ray is directly related to the normal surface velocity via the local radiation impedance Z_s ,

$$p^{\text{(mem)}}(s) = -i\omega Z_s F(s) V(0) \left(\frac{A(0)}{A(s)}\right)^{1/2} e^{i\omega\phi_s}.$$
 (21)

The amplitude factor F(s) is defined as the ratio of the normal displacement to the in-surface displacement for the membrane wave, and was derived by Norris and Rebinsky⁸ as

$$F(s) = \frac{i}{kR_0(s)} \frac{Z_m}{(Z_m + Z_s)}.$$
 (22)

According to the Sturm separation theorem (see page 223 of Ince¹⁴), if the two fundamental solutions $A_1(s)$ and $A_2(s)$ have zeros along the ray, the zeros of A_1 must alternate with those of A_2 . This fact implies that the general solution A must also have zeros. Equations (19) and (21) imply that the surface fields become singular at the zeros of A. Thus the zeros of A are the caustics of the system.

In summary, the leading-order ray and ray tube equations are independent of frequency. We therefore only need to solve these equations once, and can then use the ray trajectories and tube widths at all frequencies. This is one of the greatest advantages over other numerical methods where computation must be repeated at each individual frequency. However, there are disadvantages as well. First, the surface field is singular at caustics. It has been illustrated recently by Yang et al. 10 that even on a smooth shell as simple as an ellipsoid the caustics can spread all over the surface. Hence we must deal with an infinite number of caustics on an arbitrary shell in order to construct the surface field as well as the scattered field. Second, the membrane wave contribution to the scattered response in the fluid depends upon the surface field at well defined launching points on Σ . This requires the total contribution from all the rays passing through the launching point, but finding these rays usually involves twopoint ray tracing. In other words, one must trace a sufficiently large number of the rays initiating from the coupling curve in order to find those rays which precisely pass through the launching point. The objective of this paper is to take full advantage of the pure ray method summarized above but eliminate its disadvantages through the use of the Gaussian beam method.

B. Gaussian beams on a curved surface

A Gaussian beam may be considered as a paraxial approximation of the wave field in the vicinity of a central ray. Since the central ray is confined to real space, its trajectory, denoted by position vector $\mathbf{x}_c(s)$, can be determined by solving the real ray equations (10). For convenience, we introduce a curvilinear coordinate system composed of the central ray of the beam and the geodesic perpendicular to the central ray. The central ray propagates in the direction $n=dx_c/ds$, and the perpendicular geodesic may be obtained by solving equations¹² with geodesic initial direction the $n^1 = a_3(s,0) \times n(s,0)$. Let r be the arc length along this geodesic; then a point on Σ near the central ray may be expressed as

$$\mathbf{x}(s,r) = \mathbf{x}_c(s) + r\mathbf{n}^{\perp}(s,r). \tag{23}$$

Consider a real ray initiating at the ith coupling point. The surface field along the central ray varies according to Eqs. (19) and (21). In order to extend the field away from the central ray we first expand the phase function in a paraxial manner.9

$$\phi_s(s,r) = \int_0^s \frac{dt}{c(t)} + \frac{1}{2} \mu(s) r^2$$
 (24)

[where the wavefront curvature $\mu(s)$ is defined by (13)], and then express the field in the form of a Gaussian beam:

$$p_i^{(\text{mem})}(s,r) = \gamma_i P_i(s) e^{i\omega\phi_s(s,r)}.$$
 (25)

Here and in subsequent equations the suffix i denotes the ith ray or beam. The pressure $P_i(s)$ follows from Eqs. (19) and (21) as

$$P_i(s) = P_i(0) \frac{F(s)}{F(0)} \left(\frac{A(0)}{A(s)}\right)^{1/2}$$
 (26)

Note that Eq. (25) is the same as Eq. (21) except for the additional factor γ_i , which is introduced to take into account the effect of replacing an infinite set of the surface rays by a finite number of Gaussian beams. A general expression for γ_i is given in the next subsection.

As noted above, the surface field is singular at the zeros of A(s). The only way to prevent the ray tube width from vanishing is to analytically extend the initial real wavefront curvature into complex space. That is, instead of (14)2, we take

$$\mu(0) = \mu_1(0) + i\mu_2(0), \tag{27}$$

where $\mu_1(0)$ and $\mu_2(0)$ are both real with Im $\mu_2(0) > 0$. The ray tube width and its first derivative then follow from (15) and (27) as

$$A(s) = [A_1(s) + \mu_1(0)A_2(s)] + i\mu_2(0)A_2(s), \qquad (28a)$$

$$B(s) = [B_1(s) + \mu_1(0)B_2(s)] + i\mu_2(0)B_2(s).$$
 (28b)

Since $A_1(s)$ and $A_2(s)$ cannot vanish at the same point, the magnitudes of the parameters A(s) and B(s), and hence the surface field (25), must remain finite and nonzero at every point along the beam. At the same time the surface wavefront curvature μ becomes complex, and may be rewritten as

$$\mu(s) = \frac{[B_1(s) + \mu_1(0)B_2(s)] + i\mu_2(0)B_2(s)}{[A_1(s) + \mu_1(0)A_2(s)] + i\mu_2(0)A_2(s)}.$$
 (29)

Its imaginary part follows from Eqs. (17) and (29) as

Im
$$\mu(s) = [(A_1(s) + \mu_1(0)A_2(s))^2 + (\mu_2(0)A_2(s))^2]^{-1}\mu_2(0).$$
 (30)

The choice $\mu_2(0) > 0$ implies that Im $\mu(s) > 0$ for every arc length s, and hence the Gaussian beam preserves the character of the Gaussian profile as it travels over the shell's surface. Furthermore, the imaginary part of the complex curvature is related to the beam width, denoted by $\delta(s)$:

$$\delta(s) = [\omega \mu_2(s)]^{-1/2}.$$

The Gaussian beam solution is thus completely specified by the initial conditions for $\mu_1(0)$ and $\mu_2(0)$ [assuming A(0)] = 1]. The choice of these parameters is arbitrary, subject to the constraint that Im $\mu_2(0)>0$. In this paper we take $\mu_1(0)$ to be the real initial wavefront curvature given by Eq. (14), and choose a positive number for $\mu_2(0)$ in such a way that the initial wave field as defined by the Gaussian beam summation is smooth.

Special care must be taken in evaluation of the beam amplitude $P_i(s)$ from Eq. (26), because the square root of the complex ray tube width could be a multivalued function. In the case where $A_1(s)$ and $A_2(s)$ possess zeros along a ray, the complex number A(s) then corresponds to a curve winding around the origin in the complex plane. As A(s) goes around the origin for one complete turn, its phase is changed by 2π , resulting in a change of $-\pi$ in the phase of the amplitude $P_i(s)$. Thus determination of the phase of the complex ray tube width is essential to the application of the Gaussian beam method. It helps to express the ray tube width in the form

$$A(s) = |A(s)|e^{i\psi(s)}, \tag{31}$$

where, according to Eq. (28a), the amplitude is

$$|A(s)| = \sqrt{(A_1(s) + \mu_1(0)A_2(s))^2 + (\mu_2(0)A_2(s))^2}$$

and the phase is

$$\psi(s) - \psi(0) = \text{Im} \int_0^s \frac{A'(u)}{A(u)} du.$$
 (32)

The derivative of A(s) is related to B(s) by the variational ray equations (12), which in turn is related to the wavefront curvature μ . Also, Eq. (14)₁ implies that $\psi(0)=0$, and hence by Eqs. (12) and (13)

$$\psi(s) = \int_0^s c(u) \mu_2(u) du.$$
 (33)

Since $\mu_2(s) > 0$, the phase $\psi(s)$ must increase smoothly and monotonically with arc length. The amplitude of the ith beam in Eq. (26) therefore becomes

$$P_i(s) = P_i(0) \frac{F(s)}{F(0)} |A(s)|^{-1/2} e^{-1/2\psi(s)}.$$
 (34)

In order to illustrate the characteristic behavior of the phase of A(s), consider a Gaussian beam on a spherical shell

614

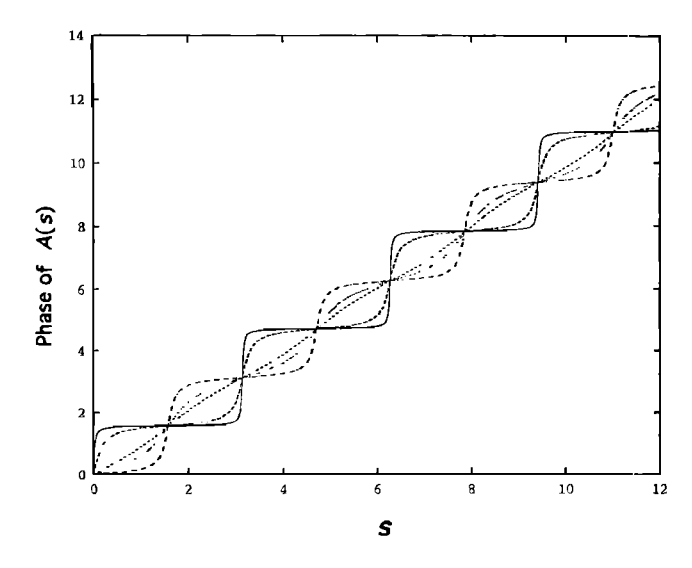


FIG. 1. The phase of complex ray tube widths as the function of the arc length along a ray traveling over the unit spherical shell. These curves correspond to the same real part of $\mu(0)$, that is, $\mu(0)=0$, but five different values of the imaginary part: $\mu_2(0)=45.85/c$ (solid), 7.34/c (long-dashed), 0.82/c (short-dashed), 0.46/c (dotted), and 0.12/c (chain-dotted).

of radius R, originating from latitude $\theta = \theta_0$ and initially directed towards the south pole ($\theta = \pi$). The central ray trajectory is a great circle; the two sets of the fundamental solutions for the ray tube width are

$$A_1(\theta) = \cos(\theta - \theta_0), \quad B_1(\theta) = -(1/cR)\sin(\theta - \theta_0),$$

$$A_2(\theta) = cR \sin(\theta - \theta_0), \quad B_2(\theta) = \cos(\theta - \theta_0),$$

and Eq. (29) reduces to

$$cR\mu(s) = \frac{cR\mu(0)\cot(\theta - \theta_0) - 1}{cR\mu(0) + \cot(\theta - \theta_0)}.$$
 (35)

Substituting Eq. (35) into Eq. (33) and then numerically evaluating the integral along the ray path gives the phase of the complex ray tube width A(s). This is plotted in Fig. 1 for five different initial values of μ_2 but the same initial value of μ_1 , i.e., $\mu_1(0)=0$. These curves show that the phase is a smooth function defined everywhere, even at caustics. As $\mu_2(0)$ increases from 0.12/c to 45.85/c, the phase deforms continuously from a smooth staircase function into a straight-line function and then into another staircase function. In all these cases, however, the change in phase, when the ray travels on the sphere for a half-turn, is approximately π , so that the phase of the amplitude $P_i(s)$ has a change of $-\pi/2$ according to Eq. (34). In this way the Gaussian beam solution retains all the physical properties of the pure ray solution while smoothing out the discontinuities and singularities.

C. Synthesis of the surface field along a curve

The only undetermined parameter in the Gaussian beam solution (25) is the factor γ , which results from the decomposition of the continuous wave field into a finite number of Gaussian beams along the coupling curve. In fact, the decomposition and superposition of Gaussian beams are two aspects of the same problem. We first consider the general

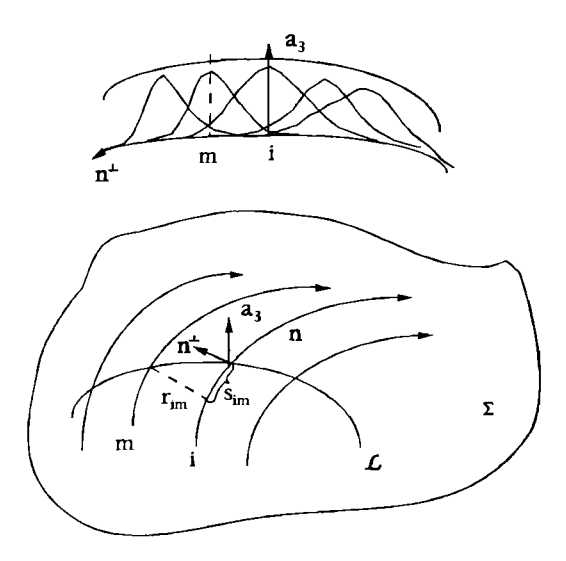


FIG. 2. Decomposition of a continuous wave field into a finite number of Gaussian beams on an arbitrarily curved surface.

issue of synthesizing the surface field along a given smooth curve using Gaussian beam solutions. We will then consider the superposition along the coupling curve as a special case and derive the general expression for the factor γ. Similar problems have been discussed in some detail by Červený et al., Nowack and Aki, and White et al. All of these previous treatments are limited to Euclidean space and most of their results are not directly applicable to non-Euclidean space, i.e., a curved surface.

In order to synthesize the wave field on a smooth curve \mathscr{L} arbitrarily given on the shell's surface, as shown in Fig. 2, we need only consider the contribution from each Gaussian beam that intersects \mathscr{L} . Beams that do not intersect the curve and are also sufficiently far away from \mathscr{L} will have little effect on the field on it. We only consider contributions from the first intersection, although the effects of subsequent ray crossings of \mathscr{L} can be evaluated in a similar manner. Points on the curve \mathscr{L} may be expressed in the parametric form $\mathbf{x}_l = \mathbf{x}_l(t)$, where t is the arc length with respect to a fixed point on \mathscr{L} . Suppose there are N ray intersection points along \mathscr{L} , specified by $\{t_i, i=1,2,...,N\}$. The Gaussian beams are labeled according to the indices of the intersection points along \mathscr{L} . The arc lengths of the central rays at the points of intersection are denoted by $\{\varphi_i, i=1,2,...,N\}$.

Now let us consider the local expansion of the curve \mathcal{L} in the central ray coordinate system of the *i*th beam, $\{\mathbf{n}_i, \mathbf{n}_i^1, \mathbf{a}_3\}$,

$$\mathbf{x}_{l}(t) = \mathbf{x}_{l}(t_{i}) + \dot{\mathbf{x}}_{l}(t_{i}) \Delta t_{i} + \frac{1}{2} \ddot{\mathbf{x}}_{l}(t_{i}) (\Delta t_{i})^{2}, \tag{36}$$

where $\Delta t_i = t - t_i$, $\dot{\mathbf{x}}_l$ and $\ddot{\mathbf{x}}_l$ are the first and the second derivative of the position vector on \mathcal{L} with respect to the arc length t. Thus $\dot{\mathbf{x}}_l(t_i)$ is the unit tangent vector and $\ddot{\mathbf{x}}_l(t_i)$ is the curvature vector of the curve \mathcal{L} at the *i*th intersecting point. More explicitly,

$$\dot{\mathbf{x}}_l(t_i) = \mathbf{t}, \quad \ddot{\mathbf{x}}_l(t_i) = -\kappa_1^{(i)} \mathbf{n}_i - \kappa_2^{(i)} \mathbf{n}_i^{\perp} - \kappa_3^{(i)} \mathbf{a}_3, \tag{37}$$

where $\kappa_1^{(i)}$, $\kappa_2^{(i)}$, and $\kappa_3^{(i)}$ are the components of the curvature vector of \mathcal{L} with respect to the central ray coordinate frame $\{\mathbf{n}_i, \mathbf{n}_i^1, \mathbf{a}_3\}$. The minus sign is required for consistency be-

tween the definition of the curvature on \mathcal{L} and that of the wavefront curvature μ . Therefore the central ray coordinates for a point at $\mathbf{x}_l(t)$, denoted here by (s_i, r_i) , follow from Eqs. (36) and (37) as

$$s_i(t) \approx \varphi_i + \mathbf{t} \cdot \mathbf{n}_i \Delta t_i - \frac{1}{2} \kappa_1^{(i)} (\Delta t_i)^2,$$
 (38a)

$$r_i(t) \approx \mathbf{t} \cdot \mathbf{n}_i^{\perp} \Delta t_i - \frac{1}{2} \kappa_2^{(i)} (\Delta t_i)^2$$
. (38b)

These local expressions provide an approximation to the curve \mathcal{L} in the vicinity of the ith intersection point. More precisely, $\Delta t_i \ll \sqrt{R_L}$, where R_L is the radius of the curvature of the curve \mathcal{L} , which is assumed to be much larger than the wavelength, i.e., $R_L \gg \lambda$. When $\Delta t_i \sim \sqrt{R_L}$, the expansions (38) are less accurate, but we can still use them because the Gaussian amplitude is exponentially small in this range and the error introduced by the approximation is almost negligible.

The total surface field at the point $x_l(t)$ is a sum of the contributions from each Gaussian beam solution (25). That is,

$$P(\mathbf{x}_l(t)) = \sum_{i=1}^{N} \gamma_i P_i(s_i) \exp\left[i\omega \left(\frac{s_i}{c} + \frac{1}{2}\mu(s_i)r_i^2\right)\right]. \quad (39)$$

We now specialize this to the case when the curve \mathcal{L} coincides with the coupling curve \mathcal{L} . The surface field at every point on \mathcal{L} is given by Eq. (26) with s=0, so that the left-hand side of Eq. (39) is known. The only unknowns are the factors γ_i with i=1,2,...,N, which can be determined by collocation at specified points of \mathcal{L} . That is, we match the known field to the superposition of Gaussian beams at each coupling point, or equivalently, at the N points of intersection $\mathbf{x}_i(t_i)$, i=1,2,...,N, of the curve \mathcal{L} with the central rays. Applying the collocation procedure to Eq. (39) yields a system of linear algebraic equations for the unknowns γ_i ,

$$P_{m}(t_{m}) = \sum_{i=1}^{N} \gamma_{i} P_{i}(t_{i}) \exp \left[i\omega \left(\frac{s_{im}}{c} + \frac{1}{2} \mu(s_{i}) r_{im}^{2} \right) \right],$$

$$m = 1, 2, ..., N,$$
(40)

where $s_{im} = s_i(t_m)$ and $r_{im} = r_i(t_m)$ are the coordinates of the point $\mathbf{x}_i(t_m)$ in the central ray coordinate system of the *i*th beam, and $s_i = s_i(t_i)$.

In order to be more explicit, we consider the case when the coupling curve is also the initial wavefront, as on a spherical shell. Then, $\varphi_i=0$, and to a first approximation the amplitudes $P_i(t_{im})$ and initial wavefront curvatures are constants. For simplicity, we consider the case where N beams are equally spaced along the coupling curve with Δt as the distance between two central rays of two neighboring beams, so that $t_m - t_i = (m - i)\Delta t$. It is then reasonable to assume that the weights γ_i are also constant. An explicit expression can be found using the identities $\dot{\mathbf{x}}_l \cdot \mathbf{n} = \ddot{\mathbf{x}}_l \cdot \mathbf{n}^\perp = 0$ and $\dot{\mathbf{x}}_l \cdot \mathbf{n}^\perp = 1$, and the simplified form of Eqs. (38) for the ray coordinates of the mth coupling point in the coordinate system of the ith beam,

$$r_i(t_m) = t_m - t_i, \quad s_i(t_m) = -(\kappa_1/2)(t_m - t_i)^2.$$
 (41)

Thus using the fact that the curve is closed and therefore periodic in t, we have that

$$\gamma_i = \eta \Delta t \sqrt{k \alpha_0 / 2 \pi},\tag{42}$$

where

$$\eta = \left\{ \frac{1}{\sqrt{\pi}} \sum_{m=1}^{N} \exp\left(-\frac{1}{2} k \alpha_0 (m \Delta t)^2\right) \sqrt{\frac{k \alpha_0}{2}} \Delta t \right\}^{-1}$$
(43)

and

$$\alpha_0 = c \,\mu_2(0) - i(c \,\mu_1(0) - \kappa_1). \tag{44}$$

When the number of beams is sufficiently large, i.e., $N \ge 1$, the sum in Eq. (43) may be approximated by a Gaussian integral, so that

$$\eta = \left\{ \frac{1}{\sqrt{\pi}} \int_{\mathcal{E}} \exp\left(-\frac{1}{2} k \alpha_0 t^2\right) \sqrt{\frac{k \alpha_0}{2}} dt \right\}^{-1} = 1.$$

When N is not that large we have $\eta \ge 1$.

In general, the coupling curve is not the initial wavefront, and one has to solve the system of linear equations (40) for the unknown factors γ_i , i=1,2,...,N. Once these are determined, the Gaussian beam solutions for the membrane waves are completely determined by Eqs. (25) and (26).

II. CONSTRUCTION OF THE SCATTERED FIELD

We are concerned with evaluating the far-field scattering amplitude, defined as

$$\mathscr{T} = \lim_{|\mathbf{x}| \to \infty} \left(\frac{2|\mathbf{x}| p^{\text{sc}}(\mathbf{x})}{R_{\text{min}} P_0} e^{-ik_f |\mathbf{x}|} \right), \quad \text{for a finite scatter,}$$
(45)

where P_0 is the amplitude of the incident wave. The total scattered field $p^{\rm sc}$ may be approximately decomposed into a specular field $p^{\rm sc(0)}$, generated by direct reflection from the shell's surface Σ , and the leaky wave field $p^{\rm sc(1)}$, which is the radiation from the membrane waves traveling over Σ ,

$$p^{\mathrm{sc}}(\mathbf{x}) \approx p^{\mathrm{sc}(0)}(\mathbf{x}) + p^{\mathrm{sc}(1)}(\mathbf{x}). \tag{46}$$

Alternatively, the total scattered response can be expressed as a Helmholtz integral,

$$p^{\text{sc}}(\mathbf{x}) = \int_{\Sigma} [G(\mathbf{x}, \mathbf{X}) \mathbf{a}_3 \cdot \nabla p^{\text{sc}}(\mathbf{X}) - p^{\text{sc}}(\mathbf{X}) \mathbf{a}_3 \cdot \nabla G(\mathbf{x}, \mathbf{X})] d\Sigma(\mathbf{X}), \tag{47}$$

where G is the free-space Green's function,

$$G(\mathbf{x}, \mathbf{X}) = -\frac{e^{ik_f|\mathbf{x} - \mathbf{X}|}}{4\pi|\mathbf{x} - \mathbf{X}|}.$$
 (48)

We will apply the Helmholtz integral to each part of p^{sc} separately in the next subsections.

A. The specular field

The specular field has been studied extensively in the last two decades. A general asymptotic expression can be found in the paper by Kachalov, 16 who derived specular and

penumbral approximations which include both bending and membrane effects. For simplicity, we neglect the bending terms in Kachalov's solution. ¹⁶ Under this approximation, the pressure generated by the specular reflection of a plane wave in the illuminated region of Σ reduces to ^{1,16}

$$p^{\operatorname{sc}(0)}(\mathbf{X}_0) = P_0 \mathcal{R}(\theta^{\operatorname{in}}), \quad \mathbf{X}_0 \in \Sigma.$$
(49)

Here, \mathbf{n}^{sc} is the direction of specular reflection, and $\mathcal{R}(\theta)$ is the acoustic reflection coefficient,

$$\mathcal{R}(\theta) = (Z_m - Z_f(\theta))/(Z_m + Z_f(\theta)), \tag{50}$$

where Z_f is defined in Eq. (4)₃. For a finite scatter, the farfield contribution to the scattered response can be obtained by substituting the specular field (49) into the Helmholtz integral (47) and using the stationary phase approximation, with the result¹⁶

$$p^{\text{sc}(0)}(\mathbf{x}) = \frac{p^{\text{sc}(0)}(\mathbf{X}_0)}{2K^{1/2}|\mathbf{x}|} e^{ik_f(|\mathbf{x}| - \mathbf{n}^{\text{sc}} \cdot \mathbf{X}_0)}.$$
 (51)

Here, X_0 is the reflection point which satisfies

$$\mathbf{n}^{\mathrm{sc}}(\mathbf{X}_0) \cdot \mathbf{a}_3(\mathbf{X}_0) = -\mathbf{n}^{\mathrm{in}} \cdot \mathbf{a}_3(\mathbf{X}_0). \tag{52}$$

The specular contribution to the far-field scattering amplitude then follows from Eqs. (45) and (51) as

$$\mathscr{F}^{\text{sc}(0)}(\mathbf{x}) = \frac{\mathscr{R}(\theta^{\text{in}})}{R_{\text{min}}K^{1/2}} e^{-ik_f \mathbf{n}^{\text{sc}} \cdot \mathbf{X}_0}.$$
 (53)

Equations (45) and (51) are valid as they stand for finite Gaussian curvature, i.e., $K \neq 0$, in the illuminated region.

The specular field becomes singular on regions with K=0, as on a circular cylinder, where a uniform theory is needed to account for the "bright lines" produced. We will not pursue this here, except to note that the analogous 2-D expression for the specular field is given in Norris. Beyond the illuminated region, the expression of the specular field becomes complicated, and detailed discussions can be found in Kachalov. ¹⁶

B. The leaky wave field

The membrane wave field is a sum over Gaussian beam solutions, and hence the linearity of the problem suggests that we represent the leaky wave field in the same manner. Thus the response for a given type of leaky wave (longitudinal or shear) is

$$p^{\text{sc}(1)}(\mathbf{x}) = \sum_{i=1}^{N} p_i^{\text{sc}(1)}(\mathbf{x}), \tag{54}$$

where

$$p_i^{\text{sc(1)}}(\mathbf{x}) = P_i^{\text{sc(1)}} e^{ik_f \phi_f}$$
 (55)

is the field radiated by the *i*th Gaussian beam. Substitution of Eq. (54) into Eq. (47) yields

$$p_i^{\text{sc}(1)}(\mathbf{x}) = \int_{\Sigma} [G(\mathbf{x}, \mathbf{X}) \mathbf{a}_3 \cdot \nabla p_i^{\text{sc}(1)}(\mathbf{X}) - p_i^{\text{sc}(1)}(\mathbf{X}) \mathbf{a}_3 \cdot \nabla G(\mathbf{x}, \mathbf{X})] d\Sigma(\mathbf{X}).$$
 (56)

The pressure gradient may be approximated as

$$\nabla P_i^{\text{sc}(1)}(\mathbf{x}) = ik_f(\nabla \phi_f) P_i^{\text{sc}(1)} e^{ik_f \phi_f} + (\nabla P_i^{\text{sc}(1)}) e^{ik_f \phi_f}$$

$$\approx ik_f(\nabla \phi_f) P_i^{\text{sc}(1)} e^{ik_f \phi_f}, \tag{57}$$

for $k_f R_{min} \gg 1$, while the gradient of the phase function defines the radiation direction, i.e.,

$$\mathbf{n}_f = \nabla \phi_f. \tag{58}$$

Then, using the continuity condition for the pressure on the shell's surface,

$$P_i^{\text{sc}(1)}e^{ik_f\phi_f} = \gamma_i P_i(s)e^{i\omega\phi_s(s,r)}, \quad \text{on } \Sigma,$$
 (59)

and substituting from Eqs. (25), (26), (48), (57), (58), and (59) into Eq. (56), we obtain

$$p_i^{\text{sc}(1)}(\mathbf{x}) \approx ik_f \gamma_i \frac{P_i(0)}{F(0)} \int_0^{+\infty} \frac{F(s) \exp(i \int_0^s k dt)}{(A(s))^{1/2}} ds$$

$$\times \int_0^{+\infty} G(\mathbf{x}, \mathbf{X}) \mathbf{a}_3 \cdot (\mathbf{n}_f + \hat{\mathbf{x}}) e^{i\omega\mu r^2/2} dr. \quad (60)$$

Here, $\hat{\mathbf{x}}$ is the unit vector in the observation direction, $\hat{\mathbf{x}} = \mathbf{x}/|\mathbf{x}|$, and the far-field condition $|\mathbf{x}| > R_{\min}$ has been used in the approximation of Helmholtz integral.

1. Reduction to a line integral

The double integral in Eq. (60) can be simplified by taking advantage of the localized nature of the Gaussian beam solution in the vicinity of the central ray. Thus only the field on or near the central ray gives an appreciable contribution to the far field. Suppose the central ray trajectory is represented by the position vector \mathbf{X}_c ; then a nearby point off the ray may be written in a form similar to Eq. (23),

$$\mathbf{X}(s,r) = \mathbf{X}_{c}(s) + r\mathbf{n}^{\perp}(s,r). \tag{61}$$

Hence

$$|\mathbf{x} - \mathbf{X}(s,r)| \approx |\mathbf{x} - \mathbf{X}_c(s)| - \hat{\mathbf{x}} \cdot \mathbf{n}^{\perp} r - \frac{1}{2} \hat{\mathbf{x}} \cdot \mathbf{n}^{\perp} r^2, \tag{62}$$

and consequently the 3-D Green's function may be expanded near the central ray as

$$G(\mathbf{x}, \mathbf{X}) = G(\mathbf{x}, \mathbf{X}_c) \exp\{-ik_f(\hat{\mathbf{x}} \cdot \mathbf{n}^{\perp} r + \frac{1}{2}\hat{\mathbf{x}} \cdot \mathbf{n}^{\perp}_{,r} r^2)\}.$$
(63)

Substitution of Eq. (63) into Eq. (60) yields

$$p_{i}^{\text{sc}(1)}(\mathbf{x}) \approx ik_{f}\gamma_{i} \frac{P_{i}(0)}{F(0)} \int_{0}^{+\infty} \frac{F(s)\exp(i\int_{0}^{s}kdt)}{(A(s))^{1/2}} \times G(\mathbf{x}, \mathbf{X}_{c})ds \int_{-\infty}^{+\infty} \mathbf{a}_{3} \cdot (\mathbf{n}_{f} + \hat{\mathbf{x}})\exp\left\{ik_{f}\left(-\hat{\mathbf{x}} \cdot \mathbf{n}^{\perp} r\right) - \frac{1}{2}\hat{\mathbf{x}} \cdot \mathbf{n}_{,r}^{\perp} r^{2} + \frac{1}{2}c_{f}\mu r^{2}\right\} dr.$$

$$(64)$$

Assuming that the pre-exponential term is independent of r, the r integral in Eq. (64) reduces to a simple Gaussian integral which can be evaluated exactly. The normal component of \mathbf{n}_f can be approximated by phase matching between the acoustic and surface waves along the central ray, yielding

$$\mathbf{n}_{f} \cdot \mathbf{a}_{3}|_{r=0} = \cos \theta_{0}. \tag{65}$$

Equation (64) therefore simplifies to

$$\begin{split} p_i^{\mathrm{sc}(1)}(\mathbf{x}) &\approx i k_f \gamma_i \, \frac{P_i(0)}{F(0)} \, \int_0^{+\infty} \frac{F(s) \mathrm{exp}(i \! \int_0^s k dt)}{(A(s))^{1/2}} \\ &\times (\cos \, \theta_0 \! + \! \hat{\mathbf{x}} \! \cdot \! \mathbf{a}_3) \\ &\times G(\mathbf{x}, \! \mathbf{X}_c) \, \sqrt{\frac{2 \, \pi}{-i k_f \sigma_1}} \, e^{(-i k_f / 2 \, \sigma_1) (\hat{\mathbf{x}} \cdot \mathbf{n}^\perp)^2} \, ds, \end{split}$$

where

$$\sigma_1 = c_f \mu - \hat{\mathbf{x}} \cdot \mathbf{n}_r^{\perp}. \tag{67}$$

The double integral over the surface has been reduced to a line integral along the central ray, and as a result, the computational time is substantially diminished. We note that the final term in Eq. (66) has a negative real part in its exponent, resulting in exponential decay as the observation direction moves away from the plane spanned by the surface ray direction **n** and the shell's surface normal **a**₃. This implies that only those beams with $|\hat{\mathbf{x}} \cdot \mathbf{n}^{\perp}| \leq 1$ give an appreciable contribution to the far field.

2. Further simplification of the line integral

Actual numerical tests show that the evaluation of the line integral in Eq. (66) is still a time consuming task, especially at high frequencies. This difficulty can be overcome by noting that the main contributions to the line integral should come from those points where the phase of the integrand is stationary. Consider the total phase of the integrand in the form $\exp\{i\Phi(s)\}\$, and suppose there are M distinct stationary phase points at $s = s_i^{(i)}$, i = 1, 2, ..., M, where

$$\Phi'(s_i^{(i)}) = 0. {(68)}$$

Applying the method of stationary phase to the line integral in Eq. (66) gives

$$p_{i}^{\text{sc}(1)}(\mathbf{x}) \approx \frac{-ik_{f}\gamma_{i}P_{i}(0)}{4\pi F(0)} \sum_{j=1}^{M} \frac{F(s_{l}^{(j)})e^{i\Phi(s_{l}^{(j)})}}{(A(s_{l}^{(j)}))^{1/2}} \times \frac{(\cos\theta_{0} + \hat{\mathbf{x}} \cdot \mathbf{a}_{3})}{|\mathbf{x} - \mathbf{X}_{c}(s_{l}^{(j)})|} \left(\frac{2\pi}{-ik_{f}\sigma_{1}}\right)^{1/2} \left(\frac{2\pi}{-i\Phi''(s_{l}^{(j)})}\right)^{1/2}.$$
(69)

The problem is to determine the stationary phase points and the values of Φ and Φ'' at these points.

We focus on the neighborhood of points along the central ray path where the following condition is satisfied:

$$k = k_f \hat{\mathbf{x}} \cdot \mathbf{n}$$
, at $s = s_c$. (70)

Note that the observation direction $\hat{\mathbf{x}}$ is not necessarily confined to the plane spanned by \mathbf{n} and \mathbf{a}_3 . Condition (70) is therefore similar to but not exactly the same as the phase matching condition of pure ray theory, for which $\hat{\mathbf{x}}$ is constrained to this plane. Equation (70) may have a number of roots along the central ray, at $s_c = s_c^{(i)}$, i = 1, 2, 3, ..., M. The Taylor expansion of the total phase in the integrand of Eq. (66) near a typical point, $s = s_c^{(i)}$, may be expressed as

$$\Phi(s) \approx \Phi(s_c^{(i)}) + \Phi'(s_c^{(i)})(s - s_c^{(i)}) + \frac{1}{2}\Phi''(s_c^{(i)})(s - s_c^{(i)})^2.$$
(71)

The position of the stationary point $s = s_i^{(i)}$ follows from Eqs. (68) and (71) as

$$s_l^{(i)} = s_c^{(i)} - \frac{\Phi'(s_c^{(i)})}{\Phi''(s_c^{(i)})},\tag{72}$$

and the phase there is, from Eqs. (71) and (72),

$$\Phi(s_l^{(i)}) = \Phi(s_c^{(i)}) - \frac{\Phi'^2(s_c^{(i)})}{2\Phi''(s_c^{(i)})}.$$
 (73)

The precise form of the total phase $\Phi(s)$ follows from Eq. (66) as

$$\Phi(s) = \int_0^s k dt + k_f |\mathbf{x} - \mathbf{X}_c(s)| - \frac{k_f}{2\sigma_1} (\hat{\mathbf{x}} \cdot \mathbf{n}^\perp)^2$$

$$\approx \int_0^s k dt + k_f |\mathbf{x}| - k_f \hat{\mathbf{x}} \cdot \mathbf{X}_c(s) - \frac{k_f}{2\sigma_1} (\hat{\mathbf{x}} \cdot \mathbf{n}^\perp)^2, \quad (74)$$

where the latter approximation applies specifically to the farfield $|\mathbf{x}| \gg |\mathbf{X}_c|$. According to Eq. (66) nontrivial contributions to the far field arise only from those rays along which $|\hat{\mathbf{x}} \cdot \mathbf{n}^{\perp}| \leq 1$. The leading-order expansions along these rays of the first and the second derivatives of $\Phi(s)$ at $s = s_c^{(i)}$ can be obtained by differentiating Eq. (74), yielding

$$\Phi'(s_c^{(i)}) \approx -\frac{k_f}{\sigma_1} (\hat{\mathbf{x}} \cdot \mathbf{n}^{\perp}) (\hat{\mathbf{x}} \cdot \mathbf{n}_{,s}^{\perp}), \tag{75a}$$

$$\Phi''(s_s^{(i)}) \approx -k_f \hat{\mathbf{x}} \cdot \mathbf{n}_s - (k_f/\sigma_1)(\hat{\mathbf{x}} \cdot \mathbf{n}_s^{\perp})^2, \tag{75b}$$

where condition (70) has been used. The directions \mathbf{n} and \mathbf{n}^{\perp} are, by definition, geodesics, and so their curvature vectors must be parallel to the normal to Σ . A simple calculation shows that

$$\mathbf{n}_{,s} = -\frac{1}{R_{\parallel}} \mathbf{a}_{3}, \quad \mathbf{n}_{,r}^{\perp} = -\frac{1}{R_{\perp}} \mathbf{a}_{3}, \quad \mathbf{n}_{,s}^{\perp} = -\frac{1}{R_{T}} \mathbf{a}_{3}, \quad (76)$$

where R_{\parallel} , R_{\perp} , and R_{T} are defined by Eq. (6).

We note that Eq. (70), combined with $|\hat{\mathbf{x}} \cdot \mathbf{n}^{\perp}| \leq 1$, implies that

$$\hat{\mathbf{x}} \cdot \mathbf{a}_3 \approx \cos \theta_0. \tag{77}$$

Substituting from Eqs. (76) and (77) into Eq. (67) yields

$$\sigma_1 \approx c \,\mu \sin \theta_0 + \cos \theta_0 / R_\perp \,. \tag{78}$$

Then, combining Eqs. (75)–(77), and differentiating Eq. (71)twice at $s = s_i^{(i)}$, gives

$$\Phi'(s_c^{(i)}) \approx \frac{k_f}{R_T \sigma_1} \cos \theta_0 \hat{\mathbf{x}} \cdot \mathbf{n}^{\perp},$$

$$\Phi''(s_l^{(i)}) \approx \Phi''(s_c^{(i)}) \approx \frac{k_f \sigma}{R_{\parallel} \sigma_1} \cos \theta_0.$$
(79)

The parameter σ is defined as

$$\sigma = c \mu \sin \theta_0 + KR_{\parallel} \cos \theta_0, \tag{80}$$

and the identity (7) has been used.

We are now in a position to calculate the stationary phase contribution to the line integral (66). First, the total phase at the stationary point $s = s_l^{(j)}$, given by Eq. (73), follows from Eq. (79) as

$$\Phi(s_l^{(i)}) \approx \int_0^{s_{(c)}^{(i)}} k dt + k_f |\mathbf{x}| - k_f \hat{\mathbf{x}} \cdot \mathbf{X}_c(s_c^{(i)}) - \frac{k_f}{2\sigma} (\hat{\mathbf{x}} \cdot \mathbf{n}^{\perp})^2.$$
(81)

Substitution of Eq. (81) into the stationary phase approximation of (69) gives

$$p_{i}^{\text{sc(1)}}(\mathbf{x}) \approx \gamma_{i} \frac{P_{i}(0)}{F(0)} \sum_{j=1}^{M} \frac{F(s_{l}^{(j)})}{(A(s_{l}^{(j)}))^{1/2}} \exp\left(i \int_{0}^{s_{c}^{(j)}} k dt\right) \times \frac{e^{ik_{f}(|\mathbf{x}| - \hat{\mathbf{x}} \cdot \mathbf{X}_{c}(s_{c}^{(j)}))}}{|\mathbf{x} - \mathbf{X}_{c}(s_{l}^{(j)})|} \frac{e^{-ik_{f}/2\sigma(\hat{\mathbf{x}} \cdot \mathbf{n}^{\perp})^{2}}}{\sqrt{\sigma/(R_{\parallel} \cos \theta_{0})}}.$$
 (82)

We note that, from Eq. (80),

$$\frac{\sigma}{R_{\parallel} \cos \theta_0} = K + \frac{c \mu}{R_{\parallel}} \tan \theta_0, \tag{83}$$

which turns out to be the Gaussian curvature of the radiated wavefront at the launching point. A detailed geometrical interpretation for Eq. (83) can be found in the paper of Yang.¹⁷ Let $\rho_1^{(0)}$ and $\rho_2^{(0)}$ be the two principal radii of curvature of the radiated wavefront at the launching point; then Eq. (82) may be rewritten in a more concise form,

$$p_{i}^{\text{sc}(1)}(\mathbf{x}) \approx \sum_{j=1}^{M} (\rho_{1}^{(0)} \rho_{2}^{(0)})^{1/2} \frac{\gamma_{i} P_{i}(s_{l}^{(j)})}{|\mathbf{x} - \mathbf{X}_{c}(s_{l}^{(j)})|} \exp\left(i \int_{0}^{s_{c}^{(j)}} k dt\right) \times e^{ik_{f} ||\mathbf{x}| - \hat{\mathbf{x}} \cdot \mathbf{X}_{c}(s_{c}^{(j)})|} e^{-(ik_{f} t/2\sigma)(\hat{\mathbf{x}} \cdot \mathbf{n}^{\perp})^{2}}.$$
(84)

 $P_i(s_i^{(j)})$, given by Eq. (26), is the amplitude of the pressure at the stationary point, $s = s_i^{(j)}$, on the central ray of the *i*th Gaussian beam.

The contribution to the far-field scattering amplitude from each beam now follows from Eqs. (45) and (84) as

$$\mathcal{F}_{i} = \frac{2}{R_{\min} P_{0}} \sum_{j=1}^{M} (\rho_{1}^{(0)} \rho_{2}^{(0)})^{1/2} \gamma_{i} P_{i}(s_{l}^{(j)}) \exp\left(i \int_{0}^{s_{c}^{(j)}} k dt\right) \times e^{-ik_{f} \hat{\mathbf{x}} \mathbf{X}_{c}(s_{c}^{(j)})} e^{-(ik_{f}/2\sigma)(\hat{\mathbf{x}} \cdot \mathbf{n}^{\perp})^{2}}.$$
 (85)

It is interesting and useful to compare this approximation with the predictions of "pure ray theory" for the radiated far-field response. The latter involves only those surface rays whose directions lie exactly in the plane spanned by $\hat{\mathbf{x}}$ and \mathbf{a}_3 , and only these radiate the leaky wave field to the observation point. In contrast, the Gaussian beam solution (84) shows that virtually every beam contributes to the field at the observation point, each weighted by a Gaussian profile from the final term in Eq. (84). The far-field contributions from those beams with $\hat{\mathbf{x}} \cdot \mathbf{n}^1 = 0$ (84) reduce to the result of the pure ray theory. However, the probability of an arbitrary beam satisfying this two-point ray tracing constraint is zero, in general.

Finally, the total leaky wave field can now be calculated from the sum of each Gaussian beam solution using Eqs. (54) and (84). It is clear that the solution to the leaky wave field is uniformly valid for all observation directions.

III. NUMERICAL IMPLEMENTATION AND TEST

A. The basic ray method

The Gaussian beam methodology outlined above has been integrated into an efficient numerical scheme we developed recently. ¹⁰ The scheme is based on pure ray and wavefront theory, allowing us to trace rays on arbitrarily curved shells and to determine the associated ray amplitudes. The general procedure can be summarized briefly as follows. The first step is to divide the shell surface into a number of small quadrilateral patches. The local geometry of each path is approximated by the parametric representation

$$x_k^{(N)} = \sum_{i=1}^{p+1} \sum_{j=1}^{p+1} S_{ijk}^{(N)}(\xi^1)^{p+1-i} (\xi^2)^{p+1-j},$$

$$0 \le \xi^1, \quad \xi^2 \le 1, \tag{86}$$

where $x_k^{(N)}$, k=1,2,3, are the three covariant components of the position vector under the fixed global Cartesian coordinate system, and the superscript N denotes the patch number. The order of the polynomial is specified by the integer p, which we take for convenience as p=3, so that Eq. (86) involves bicubic spline functions. The two parameters ξ^1 and ξ^2 are treated as the local curvilinear coordinates, from which local curvilinear coordinate frames can be defined within each patch. The surface metric and curvature tensors can then be obtained from Eq. (86) by differentiation. Finally, the system of ray equations (10) and (12) are solved numerically using the fourth-order Runge-Kutta method. ¹⁸

The following subsections discuss how the Gaussian beam method can be integrated into this existing ray-based scheme, and describes the construction of the scattered field from ray tracing.

B. Constructing ray trajectories and ray tube widths

The ray tracing scheme outlined above can be used to obtain the central ray trajectories and the ray tube widths for a given shell. These quantities are independent of frequency as well as the observation directions, and there is no need to repeat the computation for every frequency or for different observation directions. In the present scheme we first store the ray results in a data file for subsequent use in computing the scattered field at all frequencies. Obviously, one can only store the coordinates and ray tube widths for a finite number of points along a ray path. The stationary point, however, may not be one of these points. We therefore need to approximate intermediate values between two adjacent points using appropriate interpolation functions. Here, we use cubic spline functions for the interpolation.

Let i_a and i_b denote the numbers of two adjacent nodal points along a ray and assume, for simplicity, that they lie within the same patch. The intermediate values of the local coordinates between i_a and i_b may then be expressed as

$$\xi^{(i)\alpha} = F_1(t)\xi^{(i_a)\alpha} + F_2(t)\xi^{(i_b)\alpha} + F_3(t)\xi^{(i_a)\alpha}_{,t} + F_4(t)\xi^{(i_b)\alpha}_{,t},$$
(87)

where

619

$$t = (s - s^{(i_a)})/l_i, \quad l_i = s^{(i_b)} - s^{(i_a)},$$

$$F_1(t) = 2t^3 - 3t^2 + 1, \quad F_2(t) = F_1(1 - t) = -2t^3 + 3t^2,$$

$$F_3(t) = t^3 - 2t^2 + t, \quad F_4(t) = F_3(1 - t) = t^3 - t^2.$$

It follows from the ray equations (10) that

$$\xi_{l}^{(i_a)\alpha} = l_i n^{(i_a)\alpha}, \quad \xi_{l}^{(i_b)\alpha} = l_i n^{(i_b)\alpha}, \tag{88}$$

and so Eq. (87) becomes

$$\xi^{(i)\alpha} = F_1(t)\xi^{(i_a)\alpha} + F_2(t)\xi^{(i_b)\alpha} + F_3(t)l_i n^{(i_a)\alpha} + F_4(t)l_i n^{(i_b)\alpha}.$$
(89)

Differentiating this equation with respect to arc length yields the intermediate values of the components of the tangent vector along the ray.

$$n^{\alpha} = F_1'(t) \xi^{(i_a)\alpha} / l_i + F_2'(t) \xi^{(i_b)\alpha} / l_i + F_3'(t) n^{(i_a)\alpha} + F_4'(t) n^{(i_b)\alpha}.$$
(90)

The ray tube width can also be interpolated in a form similar to Eq. (89) by using Eqs. (12):

$$A(s) = F_1(t)A^{(i_a)} + F_2(t)A^{(i_b)} + F_3(t)l_i c B^{(i_a)} + F_4(t)l_i c B^{(i_b)}.$$
(91)

In the present numerical scheme we store the data for $A_1(s)$ and $A_2(s)$ instead of A(s), but the expression in (91) remains unaltered.

C. Finding the stationary phase points

The positions of the stationary points $s_l^{(i)}$ along a central ray are defined by Eq. (72), which in turn depend on the roots of Eq. (70) or, equivalently,

$$\hat{\mathbf{x}} \cdot \mathbf{n} = \sin \theta_0. \tag{92}$$

Although the roots to this equation are easy to find, in principle, numerical experience shows that some roots can be missed due to numerical errors in the ray trajectory. This is not a major problem, and can always be avoided with sufficiently close gridding. In practice, we employ an alternative strategy for finding these roots, which we describe next. We first note that the same difficulty does not occur in solving Eq. (3) for the coupling points, even when a less accurate approximation of the shell's surface is employed. The explanation is that the normal vector a3 is defined continuously over the surface, and the roots of Eq. (3) form a continuous curve, whereas the ray direction n is defined along a curve, and as a result the roots of Eq. (92) are isolated points. Conceivably, numerical errors may shift a root from its exact position. Although such a shift only slightly distorts the coupling curve, it could move a root of (92) away from the ray and thus result in the root being missed. Enlightened by this observation, we rephrase the condition (92) into a form similar to the coupling condition [see Eq. (2)₁],

$$\hat{\mathbf{x}} \cdot \mathbf{a}_3 = \cos \theta_a. \tag{93}$$

The angle θ_e between the directions of $\hat{\mathbf{x}}$ and \mathbf{a}_3 at the point $s = s_c$ is related to the critical angle by

$$\cos \theta_e = \sqrt{1 - (\hat{\mathbf{x}} \cdot \mathbf{n})^2 - (\hat{\mathbf{x}} \cdot \mathbf{n}^{\perp})^2} = \sqrt{\cos^2 \theta_0 - (\hat{\mathbf{x}} \cdot \mathbf{n}^{\perp})^2},$$
(94)

with the restriction $|\hat{\mathbf{x}} \cdot \mathbf{n}^{\perp}| \leq \cos \theta_0$. The procedure is therefore to find roots of

$$\hat{\mathbf{x}} \cdot \mathbf{a}_3 = \cos \theta_0 \sqrt{1 - (\hat{\mathbf{x}} \cdot \mathbf{n}^\perp)^2 \sec^2 \theta_0},\tag{95}$$

along those parts of the surface ray satisfying the simultaneous constraints

$$|\hat{\mathbf{x}} \cdot \mathbf{n}^{\perp}| \leq \cos \theta_0 \quad \text{and } \hat{\mathbf{x}} \cdot \mathbf{n} > 0.$$
 (96)

By this means we can obtain all the roots $s_c^{(i)}$, i = 1,2,3,..., in spite of small perturbations to the surface ray path induced by numerical errors.

D. Numerical test on a sphere

We now describe a numerical test of the general method for computing the far-field scattering from arbitrary, nonseparable shells. The test case is the simplest geometry—a spherical shell of radius R=1, for which both exact and ray asymptotic solutions are available. We treat the sphere as an arbitrary surface, without taking any advantage of its spherical shape. In other words, the procedure used here for the sphere is exactly the same as for an arbitrarily curved shell. The shell's surface is first meshed into 384 quadrilateral patches. The scheme developed and described in Yang et al. 10 is then used to determine the coupling curve, and to trace N=36 central rays that are initially spaced at equal intervals along the coupling curve. Each surface ray is followed for an arc length of 125 and the ray trajectories and the ray tube widths are stored. The ray data is subsequently used to reconstruct the ray paths in parametric form, and to determine the positions of the stationary points following the procedures described in the two previous subsections. The final solution for the scattered field can be computed from Eq. (82).

The initial complex wavefront curvature $\mu(0) = \mu_1(0) + i\mu_2(0)$ is an arbitrary parameter that needs to be prescribed. In principle, $\mu_1(0)$ could be any real number, and $\mu_2(0)$, associated with the beamwidth, should be chosen in such a way that the initial wave field along the coupling curve is smooth as the result of the beam summation. Actual numerical tests confirm that the choice of $\mu_1(0)$ hardly affects the final solution. Similar tests, using the 36 surface rays, also show that the initial wave field defined by the beam superposition is smooth if $0.4lc < \mu_2(0) < 2.0lc$. Based on these findings, the calculations reported here use

$$\mu_1(0) = 0, \quad \mu_2(0) = 0.82/c.$$
 (97)

The far-field scattering amplitude defined by Eq. (45) is shown in Fig. 3 for six different directions, defined by the angle θ between the backscattering and observation direction. Three curves are plotted for each θ : the Gaussian beam superposition, the exact thin shell prediction, and the ray-asymptotic solution of Norris and Rebinsky.¹

Numerical results for backscattering are shown in Fig. 3(a), and are seen to agree well with the two reference solutions over a wide frequency range. We notice some discrep-

620

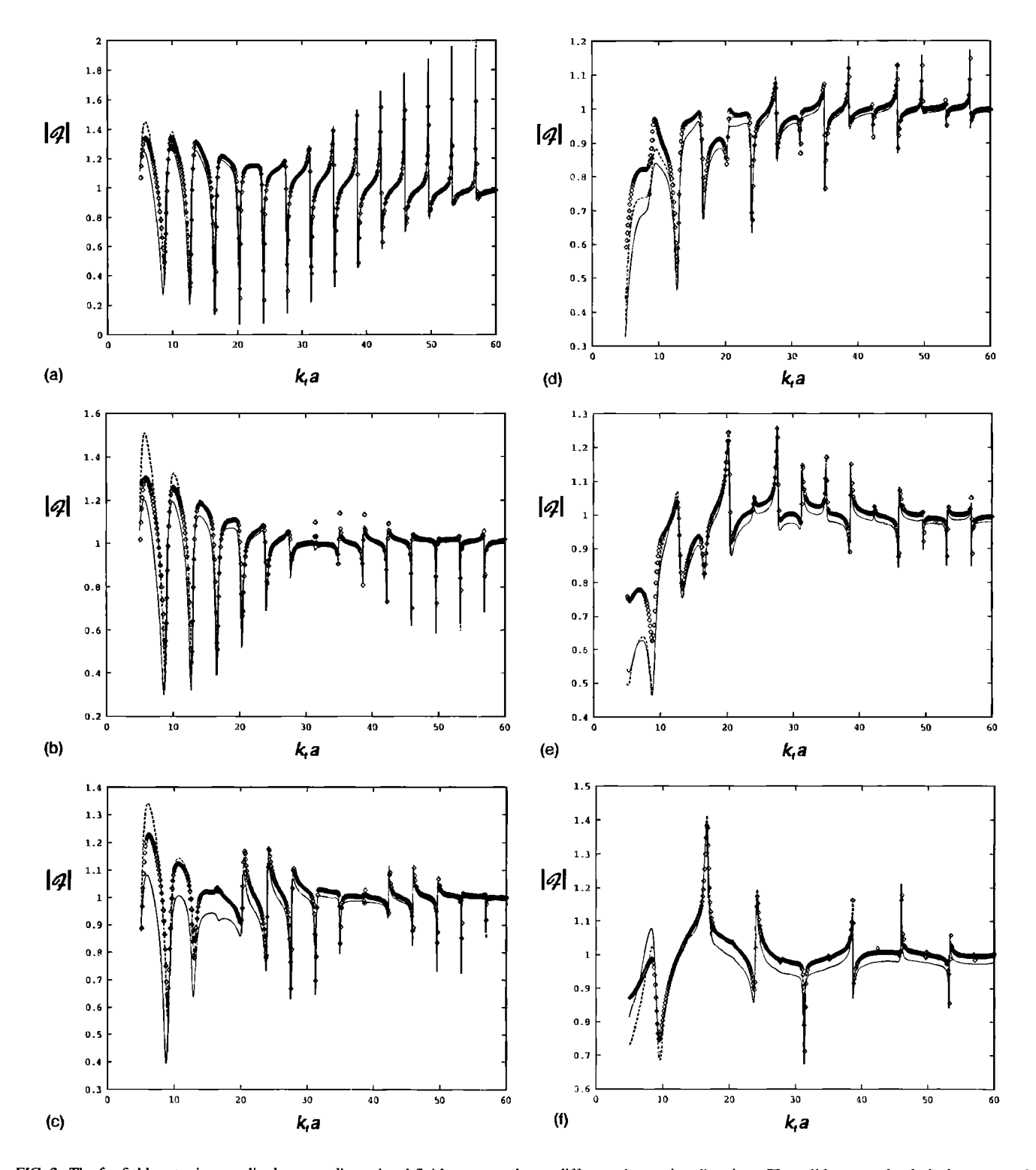


FIG. 3. The far-field scattering amplitude vs nondimensional fluid wave number at different observation directions. The solid curves, the dashed curves, and the diamonds correspond to the exact solutions, the ray-based asymptotic solutions (Ref. 1), and the present results, respectively. (a) θ =0°, (b) θ =15.82°, (c) θ =30°, (d) θ =60°, (e) θ =75°, (f) θ =90°.

ancies at the higher frequency resonances, which probably result from the truncated arc length of each beam. Thus the attenuation along a ray decreases as the frequency increases because the imaginary part in the dispersion equation (3) decreases. This suggests that we should trace rays for longer distances in order to match the resonances adequately at high frequencies. As partial confirmation we note that the ray solution of Norris and Rebinsky¹ uses rays of infinite arc

length, and matches well with the exact solution at the resonances.

Comparisons for bistatic scattering are shown in Fig. 3(b)-(f). Note that the observation angle in Fig. 3(b) is θ =15.82°, the critical angle for longitudinal membrane waves. In this case the launching point of one of the rays is at a caustic, and the surface field at that point is singular according to the pure ray theory (although the ray theory

far-field prediction of Ref. 1 is not singular at this angle). In the present formalism the surface amplitudes at caustics are always finite, and no special treatment is necessary. In general, the comparisons for various angles, in Figs. 3(b)–(f), indicate that the beam superposition results match the pure ray predictions of Ref. 1 very well. This is to be expected, especially at higher frequencies where the superposition can be shown to reproduce the ray theory exactly. There are some discrepancies between the beam superposition and the exact solution, and these discrepancies tend to propagate to higher frequencies as the observation angle increases. We believe that these discrepancies are due to the simplified approximation used for the specular field, which is not uniformly valid at all observation directions.

We note that the pure ray theory prediction of Ref. 1 for bistatic scattering is also not uniformly valid in all directions. Specifically, backscatter from a sphere requires special treatment because the number of rays reaching the observer goes from 2 to ∞ as $\theta \rightarrow 0$. One can, of course, derive uniform theories to account for the transition, but they require prior knowledge of the ray picture. In contrast, the Gaussian beam method treats backscattering exactly the same as bistatic scattering, and consequently the expression for the field radiated from the membrane waves is uniformly valid for all observation directions.

We find that the beam solution for backscattering (θ =0) is less sensitive to the number of beams used and to numerical errors in the ray paths and the ray tube widths. This is because, in backscatter, each beam makes an equal contribution to the far field and the errors are averaged out in the Gaussian beam summation. For bistatic scattering, however, only those beams near the plane spanned by the incident and observation direction give appreciable contributions to the far field. In that case the accuracy of the beam method is more sensitive to the accuracy of individual beams and the density of the beams, or the total number of beams used.

IV. CONCLUSION

The Gaussian beam summation method is normally used to model wave propagation through nonuniform media. In this paper, we have developed the first application of the method to scattering from a wave bearing object. The beams are used to model the on-surface dynamics on fluid-loaded smooth elastic shells of arbitrary shape, and also provide a natural means to calculate the scattered acoustic far field. At the same time, we have incorporated the Gaussian beam method into the ray-based scheme developed in Ref. 10. The outcome is a hybridized scheme, in which the coupling of the incident wave to the membrane waves and the subsequent wave propagation on the shell's surface are described by pure ray theory, whereas the radiation from the surface membrane waves is determined by the Gaussian beam method.

The scheme outlined here provides a new procedure for numerically solving the scattering problem for submerged elastic shells. It is closely related to pure ray theory, but has demonstrated several advantages over the ray method. First, the surface field remains finite even at caustics, which is a common feature of the Gaussian beam method. Second, the method removes the need to perform two-point ray tracing, a task which is equivalent to finding the rays that connect the launching point and the coupling point. Finally, the beam summation automatically provides a uniform result at all observation directions. There is no need to distinguish certain observation directions, as is required using pure ray theory.

The numerical comparison tests on the sphere show that the accuracy of the present scheme depends on the number of the Gaussian beams used, as well as their initial beamwidth. These two parameters are chosen in such a way that the beam summation can accurately reproduce the continuous wave field along the coupling curve. For instance, one may set $\eta=1$ in Eq. (43) and then select the values of the parameters N and $\mu_2(0)$ accordingly. In general, the numerical result depends less on $\mu_2(0)$ as N is increased. In summary, the present scheme not only provides a robust numerical tool for the study of the acoustic scattering by arbitrarily curved, smooth elastic shells, but it also allows us to extract the physical mechanisms from numerical results.

ACKNOWLEDGMENTS

The authors would like to thank Dr. Douglas A. Rebinsky for kindly providing the reference solutions shown in Fig. 3(a)–(f). This work was supported by the Office of Naval Research and U.S. Naval Research Laboratory, Washington, DC 20375-5000.

- ¹ A. N. Norris and D. A. Rebinsky, "Acoustic coupling to membrane waves on elastic shells," J. Acoust. Soc. Am. 95, 1809–1829 (1994).
- ²J. B. Keller and W. Streifer. "Complex rays with an application to Gaussian beams," J. Opt. Soc. Am. 61, 40-43 (1971).
- ³G. A. Deschamps, "Gaussian beams as a bundle of complex rays." Electron. Lett. 7, 684–685 (1971).
- ⁴L. B. Felsen, "Complex rays," Philips Res. Rep. 30, 187-195 (1975).
- ⁵ V. Červený, M. M. Popov, and I. Pšenčik, "Computation of wave fields in inhomogeneous media—Gaussian beam approach," Geophys. J. R. Astron. Soc. 70, 109-128 (1982).
- ⁶R. Nowack and K. Aki, "The two-dimensional gaussian beam synthetic method: Testing and application," J. Geophys. Res. 89, 7797-7819 (1984).
- ⁷A. N. Norris, B. S. White, and J. R. Schrieffer, "Gaussian wave packets in inhomogeneous media with curved interfaces," Proc. R. Soc. London, Ser. A 412, 93–123 (1987).
- ⁸ A. N. Norris and D. A. Rebinsky, "Membrane and flexural waves on thin shells," ASME J. Vib. Acoust. (in press).
- ⁹A. N. Norris, "Rays, beams and quasimodes on thin shell structures," Wave Motion (in press).
- ¹⁰ Y. Yang, A. N. Norris, and L. S. Couchman, "Ray tracing over smooth elastic shells of arbitrary shape," J. Acoust. Soc. Am. (submitted).
- ¹¹ A. D. Pierce, "Waves on fluid-loaded inhomogeneous elastic shells of arbitrary shape," ASME J. Vib. Acoust. 115, 384-390 (1993).
- ¹²D. J. Struik, Lectures on Differential Geometry (Dover, New York, 1968).
- ¹³J. A. Arnaud, "Hamiltonian theory of beam mode propagation," Prog. Opt. 11, 247-304 (1973).
- ¹⁴E. L. Ince, Ordinary Differential Equations (Dover, New York, 1956).
- ¹⁵B. S. White, A. N. Norris, A. Bayliss, and R. Burridge, "Some remarks on the Gaussian beam summation method," Geophys. J. R. Astron. Soc. 89, 579–636 (1987).
- ¹⁶ A. P. Kachalov, "The pattern of sound wave scattering on a convex shell," J. Appl. Math. Mech. (PMM) 43, 336-342 (1979).
- 17 Y. Yang, "Radiation and radiation impedance on fluid-loaded elastic shells of arbitrary shape," Wave Motion (in press).
- ¹⁸ W. H. Press, S. A. Teukolsky, W. T. Vetterling, and B. P. Flannery, *Numerical Recipes*, 2nd ed. (Cambridge U.P., Cambridge, 1992).
- ¹⁹ A. N. Norris and Y. Yang (unpublished).